NeuroImage 59 (2012) 1657–1667

Contents lists available at SciVerse ScienceDirect

NeuroImage

journal homepage: www.elsevier.com/locate/ynimg

The saccadic spike artifact in MEG

Christine Carl [a,b,*], Alper Açık [b], Peter König [a,b], Andreas K. Engel [a], Joerg F. Hipp [a,c,**]

[a] Department of Neurophysiology and Pathophysiology, University Medical Center Hamburg-Eppendorf, Martinistr. 52, 20246 Hamburg, Germany
[b] Institute of Cognitive Science, University of Osnabrück, Albrechtstraße 28, 49069 Osnabrück, Germany
[c] Centre for Integrative Neuroscience, University of Tübingen, Paul-Ehrlich-Str. 17, 72076 Tübingen, Germany

ARTICLE INFO

Article history:
Received 8 July 2011
Revised 8 September 2011
Accepted 12 September 2011
Available online 22 September 2011

Keywords:
MEG
EEG
Saccadic spike potential
Saccadic spike field
Extraocular muscles
Gamma band

ABSTRACT

Electro- and magnetoencephalography (EEG/MEG) are the means to investigate the dynamics of neuronal activity non-invasively in the human brain. However, both EEG and MEG are also sensitive to non-neural sources, which can severely complicate the interpretation. The saccadic spike potential (SP) at saccade onset has been identified as a particularly problematic artifact in EEG because it closely resembles synchronous neuronal gamma band activity. While the SP and its confounding effects on EEG have been thoroughly characterized, the corresponding artifact in MEG, the saccadic spike field (SF), has not been investigated. Here we provide a detailed characterization of the SF. We simultaneously recorded MEG, EEG, gaze position and electrooculogram (EOG). We compared the SF in MEG for different saccade sizes and directions and contrasted it with the well-known SP in EEG. Our results reveal a saccade amplitude and direction dependent, lateralized saccadic spike artifact, which was most prominent in the gamma frequency range. The SF was strongest at frontal and temporal sensors but unlike the SP in EEG did not contaminate parietal sensors. Furthermore, we observed that the source configurations of the SF were comparable for regular and miniature saccades. Using distributed source analysis we identified the sources of the SF in the extraocular muscles. In summary, our results show that the SF in MEG closely resembles neuronal activity in frontal and temporal sensors. Our detailed characterization of the SF constitutes a solid basis for assessing possible saccadic spike related contamination in MEG experiments.

Introduction

Electro- and magnetoencephalography (EEG/MEG) are the means for investigating neuronal dynamics non-invasively in the human brain. However, these measures are also sensitive to other physiological sources like heartbeat, muscle activity or the rotation of the eyeball during eye movements. This compound nature of EEG/MEG signals can substantially complicate the interpretation of recorded data. A detailed knowledge of the non-neural sources affecting these measures is thus critical to allow an unequivocal description of neuronal processes.

The saccadic spike is an important example of such an artifactual signal. It is observed at the onset of even tiny saccadic eye movements. The saccadic spike artifact is characterized by strong electric transients that are believed to reflect the contraction of the extraocular muscles in the orbit (Boylan and Doig, 1989a; Kovach et al., 2011; Moster and Goldberg, 1990; Riemslag et al., 1988; Thickbroom and Mastaglia, 1985; Yuval-Greenberg et al., 2008), although some studies provide evidence for cortical contributions (Balaban and Weinstein, 1985; Brooks-Eidelberg and Adler, 1992; Csibra et al., 1997). In order to account for the effect of the saccadic spike artifact on neurophysiological measurements, one needs to first understand its statistics of occurrence and second characterize its temporal, spectral, and spatial properties.

Under free viewing conditions humans perform approximately three saccadic eye movements per second. Even when attempting to fixate humans execute spontaneous miniature saccades (i.e. microsaccades and saccadic intrusions) with an average rate of one to two saccades per second (Gowen et al., 2007; Martinez-Conde et al., 2009). Importantly, saccade rate, amplitude, and direction are modulated by sensory stimulation and task demands (Engbert, 2006; Engbert and Kliegl, 2003; Gowen et al., 2005, 2007; Laubrock et al., 2005, 2010; Reingold and Stampe, 2002; Rolfs, 2009; Rolfs et al., 2008; Valsecchi et al., 2007, 2009; Yuval-Greenberg et al., 2008) and have been linked to perceptual processes (Laubrock et al., 2008; Troncoso et al., 2008; van Dam and van Ee, 2006). Moreover, the rate of eye movements is altered in clinical populations (Martinez-Conde, 2006). This makes saccades and thus saccadic spikes omnipresent features of the visual system whose occurrence is often modulated along with experimental contrasts.

The effect of the saccadic spike on EEG and intracranial EEG (iEEG) has been studied in great detail. Both, regular saccades and miniature saccades produce at their onset a biphasic transient artifact of approximately 22 ms duration referred to as the saccadic spike potential

* Correspondence to: C. Carl, Department of Neurophysiology and Pathophysiology, University Medical Center Hamburg-Eppendorf, Martinistrasse 52, 20246 Hamburg, Germany. Fax: +49 40 7410 57752.
** Correspondence to: J.F. Hipp, Centre for Integrative Neuroscience, University of Tübingen, Paul-Ehrlich-Str. 17, 72076 Tübingen, Germany.
E-mail addresses: c.carl@uke.de (C. Carl), joerg.hipp@cin.uni-tuebingen.de (J.F. Hipp).

1053-8119/$ – see front matter © 2011 Elsevier Inc. All rights reserved.
doi:10.1016/j.neuroimage.2011.09.020

(SP, Jerbi et al., 2009; Keren et al., 2010a; Kovach et al., 2011; Riemslag et al., 1988; Yuval-Greenberg et al., 2008). The topography of the SP at its first peak is characterized by a minimum at frontal electrodes and a maximum at posterior electrodes, while the potential gradient is steepest around the eyes. The amplitude values depend on the choice of the EEG reference. For the average reference as used throughout the paper, the SP is characterized by a distribution of negative electrical potential at frontal electrodes and positive potential at parietal and occipital electrodes. This distribution is inverted at the second deflection (Csibra et al., 2000; Keren et al., 2010a; Thickbroom and Mastaglia, 1985; Yuval-Greenberg et al., 2008). In iEEG, the SP is largest at medial and ventral portions of the temporal pole (Jerbi et al., 2009; Kovach et al., 2011). The topography of the SP is lateralized ipsilateral to saccade direction (Keren et al., 2010a; Kovach et al., 2011; Moster et al., 1997; Thickbroom and Mastaglia, 1985) and its amplitude depends on saccade size (Armington, 1978; Boylan and Doig, 1989b; Keren et al., 2010a; Kovach et al., 2011; Riemslag et al., 1988). The power spectrum of the SP is characterized by a broadband peak in the gamma band from roughly 30 to 120 Hz (Jerbi et al., 2009; Yuval-Greenberg et al., 2008).

Due to its spectral properties and statistics of occurrence the SP artifact resembles neuronal gamma band activity (Kovach et al., 2011; Reva and Aftanas, 2004; Schwartzman and Kranczioch, 2011; Trujillo et al., 2005; Yuval-Greenberg et al., 2008). Particularly problematic is the fact that microsaccades and regular saccades follow a characteristic inhibition–enhancement sequence after visual and auditory stimulation that is not precisely time-locked to stimulus onset. The saccadic spike artifact occurring at every saccade onset therefore mimics an induced (non-phase locked) gamma band response to stimulus presentation at parietal EEG sensors. Notably, the effect size depends on the choice of the EEG reference. Since saccade statistics change with sensory stimulation and cognitive demands, the SP's artifact signature is often modulated along with experimental contrasts. Thus, the close resemblance of the SP to neurophysiological activity in combination with stimulation and task dependent saccade statistics constitutes a serious problem for the interpretation of the EEG data. However, the detailed knowledge on the SP's temporal, spectral, and spatial properties provides a good basis to assess confounds of neuronal signals. It is now widely agreed on that any EEG study needs to carefully control for possible SP confounds (Keren et al., 2010a; Schwartzman and Kranczioch, 2011; Yuval-Greenberg et al., 2008).

The currents in neuronal and muscular tissue generating the electrical potential measured with EEG also induce a magnetic field that can be measured with MEG. MEG complements EEG with respect to its high sensitivity for tangential sources and, since magnetic fields are less distorted by the head's tissue properties, provides an excellent basis for source analysis (Hämäläinen et al., 1993). Similarly to the SP in EEG, MEG data should be confounded by a magnetic saccadic spike field (SF). It has been speculated that the saccadic spike artifact is of minor importance for MEG (Fries et al., 2008; Gruber, 2008; Schwartzman and Kranczioch, 2011) but direct evidence is missing (but see the poster of Keren et al., 2010b, at the HBM 2010 conference). Here, we measure the SF in MEG during a memory-guided delayed saccade task. We provide a detailed temporal, spatial and spectral characterization of the SF both for guided regular as well as spontaneous miniature saccades. We investigate the effects of horizontal saccade directions and saccade sizes on the amplitude and topography of the SF and compare the SF to the SP from concurrent EEG recordings. Furthermore, we estimate the origin of the SF using distributed source analysis.

Our findings demonstrate that the saccadic spike artifact may seriously confound neurophysiological signals in MEG. The detailed characterization of the phenomenon provides a solid basis for assessing possible SF confounds in future MEG experiments. Furthermore, our study constitutes the first step towards developing tools for separating the saccadic spike artifact from MEG data.

Materials and methods

Participants

Thirteen healthy volunteers participated in this study (ten female, mean age 27.5). Subjects received monetary compensation for their participation. All participants had normal or corrected-to-normal vision, and had no history of neurological or psychiatric illness. The study was conducted in accordance with the Declaration of Helsinki and informed consent was obtained from all participants prior to recordings.

Behavioral task and stimulation

Participants performed a delayed saccade task with horizontal saccades of two different amplitudes (Fig. 1). At the beginning of each trial, subjects fixated for 800 ms a blue asterisk in the center of the screen. Surrounding the asterisk, 16 Gaussian patches were regularly arranged on an inner and outer circle (distance from the asterisk: 5.5° and 11° respectively). The 4 Gaussian patches on a horizontal line in the center of the screen served as saccade targets corresponding to four experimental conditions: leftwards long and short saccades and rightwards long and short saccades. Following fixation, the central asterisk underwent a 200 ms isoluminant color change to green with a red colored marker. The position of the red marker indicated for each trial one of the four target locations and instructed the participants to prepare a saccade. If the red marker covered the inner part of an asterisk's branch it indicated a small saccade, if it covered the outer part of the asterisk's branch it indicated a large saccade. The side of

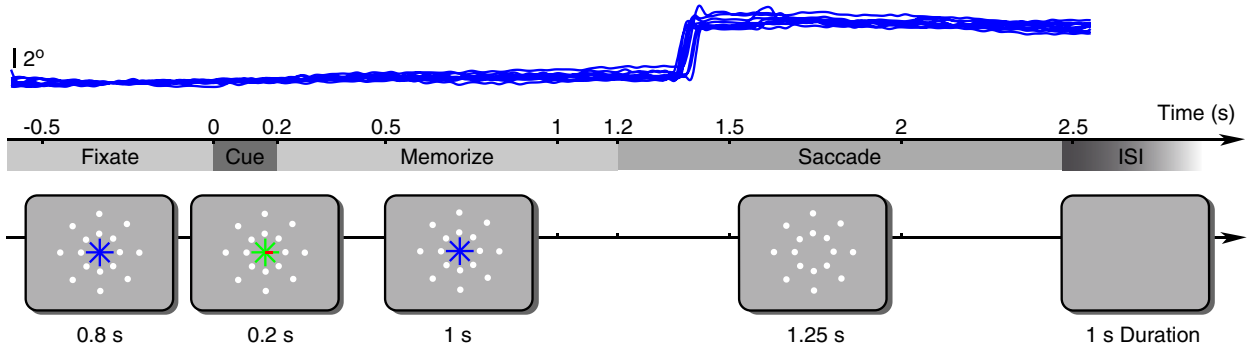

Fig. 1. Experimental task. Subjects were asked to fixate the blue asterisk in the center of the screen. An intermittent color change to green with a red marker informed about the target location for the saccade. Targets were Gaussian patches located on the horizontal line passing the center. In the depicted example, the subject was instructed to plan a saccade to the inner point on the right side. Subjects waited for 1 s until the asterisk disappeared before executing the saccade. Top: representative eye traces of one participant over the first 10 trials with a saccade to the inner right target.

the marked branch informed the participants of the saccade direction. During the following delay period of 1 s participants had to maintain fixation. Then, the asterisk disappeared. This 'go' signal instructed the subjects to perform the saccade. Subjects should maintain fixation at saccade target until it disappeared after 1.25 s. Between trials, a blank screen was presented for 1 s. In total each subject performed 500 trials (125 for each condition). Trials of all four experimental conditions were randomly presented.

During the experiment, participants were seated in the MEG chamber. Stimuli were back-projected onto the screen at 54 cm distance with a liquid crystal display video projector (Sanyo XP51 Beamer, 60 Hz refresh rate) and a two-mirror system. Stimuli were presented using the software Presentation (Neurobehavioral Systems, Albany, CA).

Analysis software

All data analyses were performed in Matlab (MathWorks, Natick, MA) with custom software and the open source toolboxes Fieldtrip (Oostenveld et al., 2011) and SPM2 (http://www.fil.ion.ucl.ac.uk/spm/).

Data acquisition and preprocessing

MEG

We recorded MEG continuously with a 275-channel (axial gradiometer) whole-head system (CTF275, VSM MedTech) in a magnetically shielded room. Two sensors were not operating resulting in a total of 273 sensors. MEG data were digitized at 1200 Hz sampling rate (300 Hz low-pass filter). Off-line, we removed line-noise with notch-filters (at 50, 100, 150 Hz), low-pass filtered the data to 170 Hz (zero phase Butterworth IIR filter, filter order 4) and down sampled it to 400 Hz.

EEG/EOG

Along with the MEG, we recorded EEG using the EEG channels of the CTF MEG system. Data were collected with an analog passband of 0.16–300 Hz at a sampling rate of 1200 Hz. We used 32 Ag/AgCL sintered flat electrodes (Easycap GmbH, Herrsching, Germany) arranged according to the 10–20 system and two electrodes at the mastoids. Additionally, we recorded a bipolar electrocardiogram and the electrooculogram (EOG) from 7 electrodes. EOG electrodes were placed over the nose, above and below each eye at the outer canthi and below the left and right eye next to the nose. Data were referenced to an electrode placed at the tip of the nose during the recording. All electrode impedances were below 15 kOhm.

Off-line, the EEG data were re-referenced to the average of the 32 EEG electrodes. The EEG and EOG were low-pass filtered (cut-off 170 Hz, zero phase Butterworth IIR filter, filter order 4). EOG data were re-referenced to the electrode Pz. For three subjects we discarded the right inner infraorbital EOG channel because of poor signal quality. We then derived the radial EOG (REOG; Keren et al., 2010a) as the average of all EOG channels.

Structural MRI acquisition

We acquired individual T1-weighted high-resolution structural images (MRI) of each subject with a 3 T Siemens MAGNETOM Trio Scanner using a coronal magnetization-prepared rapid gradient echo sequence. These MRIs were used to construct individual head models for source analysis (see below).

Eye tracker recording

Along with the neurophysiological data we recorded the eye position using an MEG compatible remote eye tracker system (iView X MEG 50 Hz, SMI, Berlin, Germany). The system monitored the right eye with an infrared camera to detect the pupil center and the cornea reflex of the infrared light source. After calibration (9 points) the system determined the gaze direction from the relative position of pupil and the corneal reflex at a rate of 50 Hz. Additionally, digitized eye traces were interpolated to match the MEG/EEG sampling rate (1200 Hz), digital to analog converted and fed to the MEG system on-line. This on-line procedure introduced temporal offsets of the eye tracker signal in relation to the MEG/EEG data. Moreover, the digital to analog conversion produced undesirable ringing artifacts. Therefore, the analog signal recorded along with the MEG/EEG just served as a coarse reference for the first alignment of the eye tracker and MEG/EEG signals.

Off-line, we aligned the digital eye tracking data to the MEG/EEG in a 2-step procedure. First, we interpolated the 50 Hz signal to 400 Hz using cubic smoothing splines and computed the cross-correlation of the interpolated digital eye tracker signal with the analog version recorded with the MEG acquisition system. Then we accounted for the offset identified by the latency of the peak in the cross-correlogram. In a second step, we refined the alignment and corrected for the offset between the EOG and the aligned eye tracker signal. To this end, we smoothed the data with a Savitzky-Golay filter (4th order, 102.5 ms) rectified and averaged all channels of both the EOG and the eye tracker signals, and estimated the offset from the peak of the cross-correlation.

To improve the quality of the eye tracker signal, we interpolated missing data. We detected periods with loss of eye tracking signal characterized by pupil size and gaze position values close to zero. If these data segments were not identified as blinks (see below) we interpolated the missing data by piecewise constant interpolation.

Artifact rejection

Trials contaminated with muscle artifacts, signal jumps or distortions of the magnetic field due to e.g. cars passing in front of the building were rejected off-line using semi-automated threshold procedures applied to the MEG signals. Since eye movements are part of the experimental design standard EOG based procedures to detect eye blinks fail. We detected eye blinks using a combination of eye tracker and EOG signals. Data with vanishing pupil diameter and fast changes in the EOG signal were identified as blink artifacts. Finally, we inspected all MEG, EEG and EOG signals manually to ensure good artifact rejection performance. On average $9.5 \pm 3.6\%$ (mean $\pm$ std) of the trials were rejected.

Data analysis

Behavioral analysis

For detection of regular saccades we employed a velocity threshold based algorithm. If coupled with a minimum saccade duration criterion this algorithm has very few parameters and is accurate in the face of stereotypical eye-movements such as those analyzed here (Salvucci and Goldberg, 2000). Because the optimal velocity threshold parameter depends on preprocessing and sampling of the recorded data as well as on saccade amplitudes, we defined the velocity threshold in a data-driven approach. We adapted the thresholds manually for the saccade amplitudes in our task (5.5º and 11º) so that saccades were detected while the number of false positives was minimized. We achieved this by visual inspection of the data, taking into account *a priori* knowledge on saccade timing. We defined periods as regular saccades in which the eye movement velocity was higher than 28.6°/s for a duration of at least 22.5 ms. Periods where the saccade velocity exceeded 53.7°/s were defined as saccades irrespective of saccade duration. We combined all saccade intervals that were less than 7.5 ms apart from each other into a single saccade interval. All other periods were labeled fixations.

The behavioral analysis revealed that subjects had a considerable variability in saccade onset and also initiated saccades before the 'go' signal. However, since this study focused on the stereotypic saccadic spike, we were not concerned about the exact timing of the saccades in general. We were only interested in ensuring that subjects performed saccades to the cued goal as instructed. To maximize the number of trials to analyze, we accepted trials with saccades that were performed

within a broad time window from 500 ms before to 770 ms after the 'go' signal. We excluded trials before 500 ms because they were unlikely to be related to the instruction and saccades later than 770 ms to ensure sufficient data following the saccade for subsequent analysis. In a next step, we rejected all trials with wrong saccade orientation or amplitude. For saccade categorization we applied drift correction at the fixation period before the cue onset (−300 ms to −100 ms) and ensured that the subjects fixated the asterisk before saccade onset within a tolerance angle of 2.3°. The saccade target was considered correct if the closest location was the cued one. Overall we discarded 13.5 ± 12.7% (mean ± std) of the trials because of faulty behavioral performance.

Additionally, we analyzed miniature saccades that occurred within the period from onset of the directional cue and onset of the guided regular saccade. We defined miniature saccades using a threshold procedure applied to the REOG: The 30–100 Hz band pass filtered REOG signal was convolved with an SP-template (provided by Keren et al., 2010a) and convoluted data segments exceeding 3 standard deviations were detected. Every detected event whose amplitude did not exceed 2° visual angle was defined as a miniature saccade. Miniature saccades occurred at an average rate of 1.45 ± 0.34 per second (mean ± std) and followed a characteristic inhibition–enhancement sequence after directional cue presentation. Note, that the low sampling rate of the eye tracker (50 Hz) did not allow reliable microsaccade detection based on eye tracker recordings.

Alignment of trials for saccadic spike characterization

Independent of saccade type or different saccade metrics, the saccadic spike is generated consistently at saccade onset (Keren et al., 2010a). However, saccade detection based on threshold procedures introduces imprecision in the estimated saccade onset and generates jitter in the timing of the saccadic spike over trials. When investigating the average SP or SF over trials we had to correct for this jitter. We aligned each trial to the first trough of the REOG within a time window of ±30 ms from detected saccade onset (Keren et al., 2010a; Kovach et al., 2011). This alignment procedure was applied to miniature and regular saccades for all analyses where we examined the temporal and spatial characteristics of the average saccadic spike.

Description of the saccadic spike on sensor level in MEG and EEG

We calculated the time course as well as the topography of the event related average of the saccadic spike for MEG and EEG. For the topographies we provide, in addition to the event related average for MEG and EEG, the root-mean-square of the SP and the planar gradient estimation of the SF for MEG. A baseline of 280 to 180 ms before saccadic onset was subtracted from the average time course of the MEG/EEG data.

The saccadic spike artifact occurs simultaneously with another eye movement related artifact—the rotation of the corneo-retinal dipole, also known as corneo-retinal potential in EEG. This rises slowly and adds to the saccadic spike artifact. It was shown that it heavily distorts the second deflection of the biphasic spike in EEG (Keren et al., 2010a; Riemslag et al., 1988). Therefore, we focused on the first deflection of the saccadic spike to study its topography. We used a baseline directly at saccade onset (7.5 ms before the first saccadic spike peak, onset was defined by the grand average time course of the eye trace). By using this single point baseline, we maximally separate the signal of the saccadic spike artifact from other signals related to saccade generation and preparation like the antecedent potential (Armington, 1978; Jagla et al., 2007; Kurtzberg and Vaughan, 1982), which starts approximately 100–150 ms before saccade onset.

We assessed statistical significance for the event related amplitude of the saccadic spike across subjects (random effects) by applying Student's *t*-test, (n = 13 with n: number of participants) at each sensor. We accounted for multiple comparisons using Bonferroni correction (alpha = 0.01, corrected for the number of sensors).

Next to event related potentials, another commonly used measure in EEG is the root-mean-square. Consequently, we additionally report this measure for the SP. In short, we calculated for each subject individually the root-mean-square of the baseline corrected event related average across the time points of the first peak of the SP (time: t > 0 ms, t < 12.5 ms, baseline: time t = 0). We present the average of the root-mean-square over subjects.

Most MEG systems use either axial or planar gradiometers to record the magnetic fields. The system we used has axial gradiometers. To provide a general description of the SF we additionally computed a planar gradient estimate for our results. To this end, we combined horizontal and vertical estimates of the planar gradient of all sensors for each subject's baseline corrected SF (Bastiaansen and Knösche, 2000). To assess where amplitude deflections of the planar gradient estimate were consistently highest across subjects, we normalized the planar gradient estimation of each subject's SF to a standard normal distribution and tested for statistical significance of the positive deflections with a one-sided Student's *t*-test over subjects (alpha = 0.01, Bonferroni corrected for the number of sensors).

For visualization we show topographies with the physical quantities (electrical potential and strength of magnetic field). These topographies are statistically masked such that values that do not reach statistical significance are presented with a semi-opaque white cover.

Lateralization of the saccadic spike artifact

We analyzed topographies of the saccadic spike for leftwards and rightward saccades separately. For this purpose we computed the saccadic spike at the time of maximal lateralization, which was derived as the maximal difference in amplitude between ipsi- and contralateral EOGs in relation to saccade direction (5 ms after saccade onset).

Spectral characteristics of the SF for regular and miniature saccades in MEG

To investigate the spectral characteristics of the saccadic spike in MEG we derived a time–frequency representation of the SF using Morlet's wavelets (Tallon-Baudry et al., 1996). The characteristic parameter for the wavelet family was, $f/\sigma_f \approx 5.8$ where σ_f is the spectral smoothing and f is the center frequency. We calculated the frequency transform at 25 logarithmically equidistant center frequencies from 16 to 128 Hz. We computed the transform for discrete time points at −100 ms to 100 ms in 10 ms steps (baseline estimated from the average at time t = −400 ms to −350 ms, in 10 ms steps, baseline for miniature saccades: t = −135 ms to −85 ms in 10 ms steps). For statistical analysis we log-transformed the power estimates to render distributions more normal and computed a Student's *t*-test on the difference in power relative to baseline over participants. Since the saccadic spike effect size is statistically weaker at a particular point in the time–frequency representation than at the peak in the time domain we used a less conservative method for multiple comparison correction. We controlled for multiple comparisons using false discovery rate (FDR) correction with q = 0.01 (Benjamini and Hochberg, 1995; Genovese et al., 2002).

Physical forward model for source analysis

To estimate neural activity at the source level, we first derived physical forward models for each subject. To this end, we defined a regular grid (0.7 cm spacing) in MNI space that comprised, in addition to the cortex, the region of the eyeballs and extraocular muscles. We affine transformed this grid into individual head space using the participants' individual MRI, and aligned the MEG sensors to the head geometry based on 3 fiducial points (nasion, left and right ear, defined in the MEG by 3 head localization coils). To derive the physical relation between sources and sensors we employed a single-shell volume conductor model (Nolte, 2003). On top of the regular grid, we computed leadfields for the center location of the extraocular

muscles. The location of the contralateral center of the extraocular muscles was used for suppression in the beamforming source analysis (see below). We defined these positions manually in the MNI template brain (Holmes et al., 1998; MNI = [−28, 38, −37] for left hemisphere, MNI = [28, 38, −37] for right hemisphere).

Source analysis of the SF using beamforming

We used adaptive linear spatial filtering (beamforming; Gross et al., 2001; Van Veen et al., 1997) with coherent source suppression (Brookes et al., 2007; Dalal et al., 2006) to estimate the amplitude of signals at the source level. The coherent source suppression approach accounts for the highly synchronized electrical activity of the extraocular muscles across the hemispheres (Kovach et al., 2011) that would otherwise lead to signal cancelation in beamforming. In short, for each source location, three orthogonal linear filters (for the three orientations at each source) were computed that pass activity from that location with unit gain and block activity from dipoles of any orientation at the location of the contralateral extraocular muscles, while maximally suppressing activity from any other source. Subsequently, the filters were linearly combined to a single filter that points to the direction of the dominant dipole (Hipp et al., 2011).

Before deriving source estimates of the SF, we band-pass filtered the event related signal by convolution with a 3-point filter to attenuate residual contributions from the corneo-retinal artifact. The 3-point filter was adapted to the temporal structure of the biphasic saccadic spike signal (filter kernel: −0.5 at −7.5 ms; 1 at 0 ms; −0.5 at 5 ms). Then, we estimated the covariance matrix that is needed for the beamforming filter from concatenated data epochs ± 30 ms around the first SF peak of all saccades. The average difference between the first peak of the SF and the baseline at the onset of the SF was then projected into source space. The absolute value served as a source estimate. This source estimate is subject to a positive bias. To account for this problem, we estimated and subtracted the bias. To this end, we randomly permuted the SF peak and SF baseline and estimated the source distribution for these data 1000 times. The average served as a bias estimate. Finally, we derived the neural activity index (NAI) of the source estimate that accounts for the spatial bias of beamforming for deep sources (Van Veen et al., 1997). For statistical analysis, we computed Student's *t*-test of the NAI at each voxel across subjects (alpha = 0.01, Bonferroni corrected for the number of voxels). Furthermore, we used a variant of beamforming for frequency domain data (Gross et al., 2001) to estimate the sources at 64 Hz at the time of saccade onset (temporal smoothing = 87 ms, frequency smoothing = 21.96 Hz). We derived a filter estimation from the real part of the cross-spectral-density matrix (cf. Hipp et al., 2011) at the time of saccade onset and baseline (t = −400 to −350 ms for regular saccades, t = −135 to −85 ms for miniature saccades) and computed the relative change of the signal power. The logarithmic transform of the average power source estimates at saccade onset and at baseline entered the statistical analysis. We tested at each voxel for significance of the difference of those power estimates over subjects using the Student's *t*-distribution (q = 0.01, FDR corrected for the number of voxels).

For visualization we overlaid the functional data onto the structural MRI of the MNI template brain, masked unsignificant values and interpolated the source data to 1 mm resolution.

Dipole fitting of the SF

To further investigate the sources underlying the lateralization of the saccadic spike of horizontal saccades we employed dipole fitting in addition to the distributed source analysis. For each subject and saccade direction, we fitted two equivalent current dipoles. We optimized the dipole orientation while dipole position was fixed to the previously defined center of the extraocular muscles (left dipole: MNI = [−28, 38, −37] and right dipole: MNI = [28, 38, −37]). Average explained variance of this dipole models was 77.43%. To summarize and visualize the subjects' individual dipole orientations, we projected each subject's normalized dipole onto a common plane. This plane was defined in the MNI template brain by the vector connecting both dipole positions and an orthogonal projection of the average orientation vector of all medial and lateral rectus muscles. We then computed the mean angle between dipoles for leftwards and dipoles for rightwards saccade trials. We tested for significant rotation of dipoles between saccades to the left and to the right using a nonparametric random permutation test (Nichols and Holmes, 2002). This had the advantage that we did not need to make any assumption about the distribution of the rotation angles. We derived a Null hypothesis distribution by 1000 times randomly permuting saccade labels 'right' and 'left' and computing the mean angle between dipoles and then determined the p-value.

Comparison of the SF and SP for miniature and regular saccades

We quantified the similarity of scalp topographies of the SF for miniature and regular saccades by computing the linear correlation across sensors. To assess differences in SF and SP amplitudes, we computed the absolute SF/SP amplitude for miniature, 5.5°, and 11° saccades at channels of interest (see inset, Figs. 7C and D) and tested for pairwise amplitude difference across subjects, using Student's *t*-test (Bonferroni corrected for 2 comparisons).

Results

The saccadic spike artifact in MEG and EEG

To investigate the effect of the saccadic spike on MEG/EEG signals we performed a delayed saccade experiment with targets at two distances (5.5°/11°) and two directions (left/right). In each trial, a directional cue instructed participants about the saccade target location. Participants memorized the location during a delay period of 1 s before they actually performed the saccade (Fig. 1).

First, we analyzed the grand average time course of the saccadic spike artifact pooled over both saccade directions and both amplitudes. To this end, we aligned the signals to saccade onset and subtracted a baseline from 280 to 180 ms before the saccade (Fig. 2A). The average saccade duration was about 50 ms, while the eye movement velocity peaked around 30 ms after saccade onset (Fig. 2A, first panel). The time course of the REOG (i.e. the average signal of all EOG channels relative to the parietal electrode 'Pz'), the EEG, and the MEG revealed a brief biphasic saccadic spike at saccade onset. The saccadic spike artifact peaked around 7.5 ms after saccade onset, inverted its polarity, and peaked again 15 ms after saccade onset (Fig. 2A, lower three panels). The second peak of the saccadic spike artifact was overlaid with the concurrent corneo-retinal artifact reflecting the rotation of the corneo-retinal dipole (Keren et al., 2010a). To isolate the SF or SP, we therefore focused the following analyses on the first deflection of the saccadic spike.

The subjects' average scalp topography of the SP in EEG was characterized by a strong negative potential of up to −16 μV at frontal sensors and a moderate positive potential of up to 8 μV at parietal sensors (Fig. 2B; average reference; $p<0.01$, Bonferroni corrected for n = 273 sensors). Accordingly, the root-mean-square of the EEG peaked at similar frontal and parietal sensors (Fig. 2C). Two sensor types are commonly used in MEG systems, axial gradiometers and planar gradiometers (Hämäläinen, 1995; Hämäläinen et al., 1993). Our MEG setup uses axial gradiometers, however, in the following description of the MEG sensor topographies we also present an estimate of the corresponding planar gradiometer representation (see Materials and methods). The SF in MEG was characterized by increases and decreases at frontal and temporal sensors for axial gradiometers (Fig. 2D; $p<0.01$, Bonferroni corrected for n = 273 sensors). The average absolute amplitudes across subjects were highest at temporal sensors reaching 14 pT. In the corresponding planar gradient representation the strongest effect of the SF was at the anterior half of the temporal

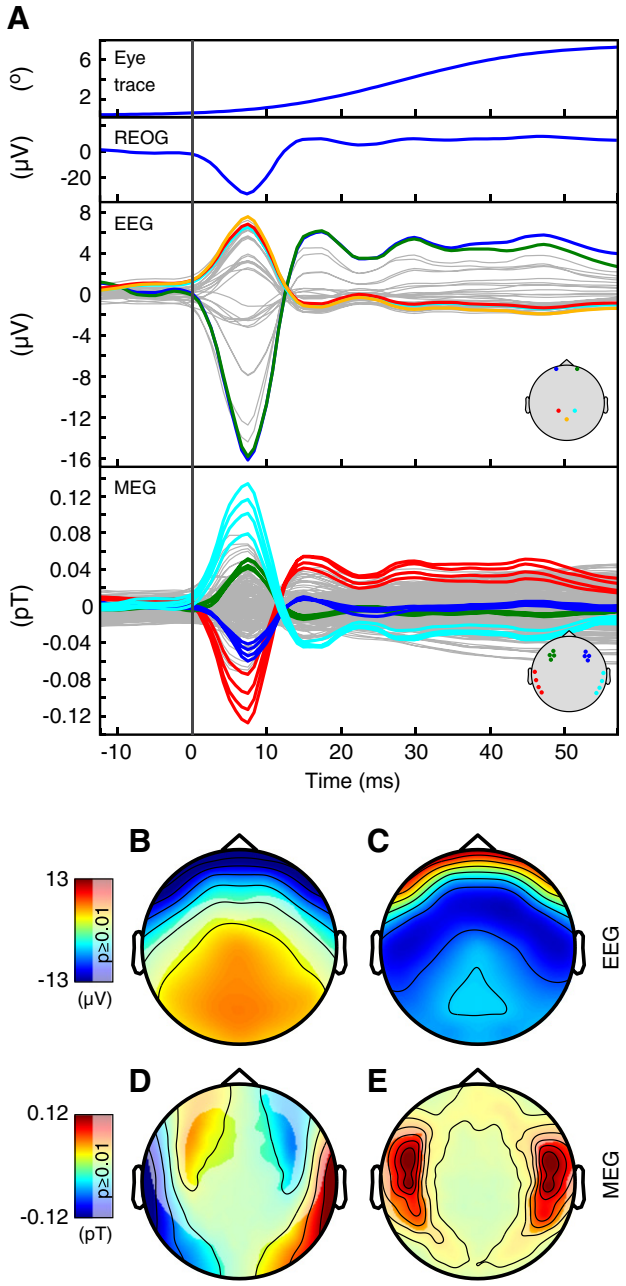

Fig. 2. SP and SF time course and topography in EEG and MEG sensor space. A. Grand average time course of baseline corrected REOG, EEG and MEG signals pooled over all saccade target locations (baseline from time t = −280 ms to −180 ms; saccade onset at time t = 0 ms). The eye trace shows the average distance from the fixation point at baseline. Trials were aligned to the first SP peak of the REOG channel (Keren et al., 2010a). Sensors for the highlighted time courses were selected according to the topographic distribution of the SP/SF potential (see B and D) and are illustrated in the insets. Time courses of all other sensors are shown in gray. B to E. Topographies of the SP/SF at the first peak of the saccadic spike (time t = 7.5 ms, indicated by the dashed line in A) baseline corrected by the signal at saccade onset (time t = 0 ms). Unmasked regions (i.e. intense color scale) in B, D and E denote significant difference to zero (*t*-test, p<0.01, Bonferroni corrected). B. Event related potential of the EEG. C. Root-mean-square of the EEG. D. Event related field for MEG axial gradiometers. E. Event related field for MEG planar gradiometer estimates.

sensors (Fig. 2E; p<0.01, Bonferroni corrected for n = 273 sensors). In conclusion, both MEG and EEG sensors were strongly affected by the saccadic spike. However, the spatial topography differed substantially. In particular, the SF in MEG did not significantly affect parietal sensors.

Source analysis of the saccadic spike

Next, we analyzed the sources of the saccadic spike. We used adaptive linear spatial filtering (beamforming) applied to the broadband SF signal. The sources were localized to the extraocular muscles of both eyes (Fig. 3A; p<0.01, Bonferroni corrected for n = 11,078 voxels). To elaborate on the spatial specificity of these sources, we omitted statistical thresholds (Fig. 3B). The activity of the sources of the saccadic spike artifact dropped from the maximum at the extraocular muscles without revealing any other prominent local maxima. Thus, source analysis using beamforming, spatially separated the SF from other neurophysiological signals into the region of the extraocular muscles.

Spectral signatures of the saccadic spike in MEG

We used time–frequency analysis to study the spectral characteristics of the saccadic spike artifact in MEG. The spectro-temporal pattern was characterized by a broadband gamma frequency range increase (~ 32 to 128 Hz) around the time of saccade onset (Fig. 4A; p<0.01, FDR corrected for n = 21 × 25 time × frequency points). The strongest power increase at 10 to 30 ms and 64 Hz was at frontal and temporal sensors. The source distribution for this frequency range was highly similar to that of the event related response (Fig. 4B; p<0.01, FDR corrected for n = 11,078 voxels; compare to Fig. 3). Thus, in line with previous EEG and iEEG studies (Kovach et al., 2011; Yuval-Greenberg et al., 2008) the saccadic spike induced signals that closely resemble neurophysiological gamma range activity in the MEG sensors.

The topography of SP and SF reflects saccade direction

Many experimental designs involve lateralized covert attention that has been shown to influence the spatial statistics of miniature saccade direction (e.g. Laubrock et al., 2010). It is therefore important to understand potential lateralization of the accompanying SP and SF, since this might induce systematic confounds in such experiments.

As a starting point, we analyzed the time course of the saccadic spike at left, central and right EOGs around saccade onset for leftwards saccades (Fig. 5A). The latencies of the first saccadic spike peak increased from ipsilateral to contralateral electrodes. However, this shift is unlikely to reflect a change in latency of the saccadic spike itself but likely reflects the corneo-retinal artifact, which adds in a spatially specific manner to the saccadic spike artifact. The corneo-retinal potential with its positive amplitude at ipsilateral and negative amplitude at contralateral EOG electrodes reduces the negative peak of the SP at ipsilateral EOGs and increases the SP at contralateral sites. Thus, while the onset and peak latency of the saccadic spike may actually remain the same, the superposition with the slowly rising corneo-retinal potential appears as a shift of the SP peak dependent on channel location. Consequently, to study the lateralization of the saccadic spike artifact as a function of saccade direction we minimized the influence of the slowly rising corneo-retinal artifact by selecting an early analysis window 2.5 ms before the saccadic spike peak. At this time, the SP topography was lateralized depending on the direction of the saccade (Fig. 5B). The negative deflection of the SP was higher at ipsilateral frontal electrodes, while the positive peak at posterior electrodes was shifted towards the side contralateral to the saccade direction.

In line with the SP in EEG, the SF in MEG was lateralized. The amplitude of the SF was significantly higher at frontal and temporal sensors ipsilateral to saccade direction (axial gradiometers; Fig. 5C, upper panel; p<0.01, Bonferroni corrected for n = 273 sensors). This finding was paralleled by a planar gradient topography with higher amplitudes at ipsilateral temporal electrodes (Fig. 5C, lower panel; p<0.01, Bonferroni corrected for n = 273 sensors). Thus, for both EEG and MEG, we found a clearly lateralized saccadic spike

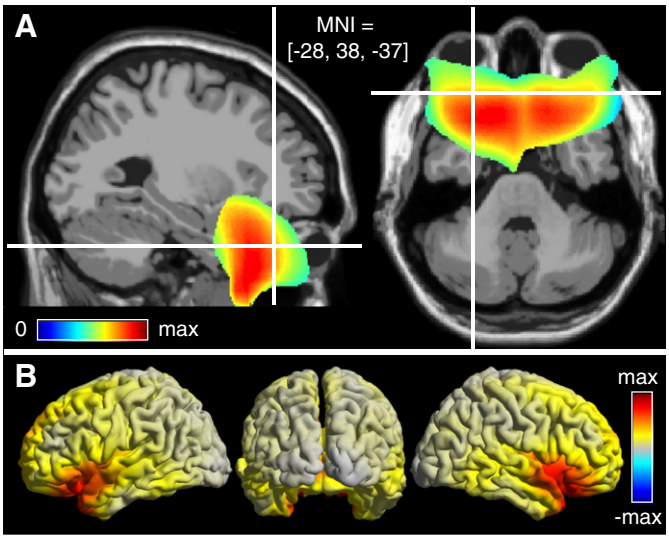

Fig. 3. SF sources in the extraocular muscles. A. Source analysis using beamforming of the first peak of the SF. The saccadic spike artifact is localized to the region of the extraocular muscles of both eyes. The average neural activity index (NAI) masked by statistics (*t*-test, $p<0.01$, Bonferroni corrected) is overlaid on the MNI template brain. B. Surface projection of the SF source without statistical mask.

artifact. This lateralization may complicate the isolation of signals of neuronal origin.

Orientation of extraocular muscle dipoles reflects saccade direction

We hypothesized that the origin of the lateralized SP/SF sensor topography is related to asymmetrical contraction of the extraocular muscles for left and right saccades. To elaborate on this hypothesis, we fitted the SF with equivalent current dipoles. We placed a dipole in the center of the extraocular muscles of each eye and optimized the orientation of these dipoles for each subject individually. Then we analyzed the orientation of the dipoles in the plane spanned by lateral and medial rectus muscles, the muscles mainly responsible for horizontal movements of the eye. We tested if the orientation of the SF dipoles changed depending on the saccade direction. Dipoles for both saccade directions were on average oriented towards the outer borders of the eyeballs. Contrasting the dipole orientation for leftwards with rightwards saccades revealed a significant rotation of 13.26° towards the ipsilateral side across subjects (Fig. 6; $p=0.01$, random permutation test). Consequently, the dipole orientation of a horizontal saccade followed the orientation of the contralateral rectus medialis and ipsilateral rectus lateralis muscle.

Comparison of SF of miniature and regular saccades

Up to this point, we studied the SP and SF at the onset of regular saccades. However, a major problem is the spike artifact related to miniature saccades that occur even under fixation. Thus, we next analyzed the SF and SP induced by miniature saccades. We extracted miniature saccades with a range of less than 2° amplitude from the fixation period of our experiment (see Materials and methods). The SF of miniature saccades had a similar topography as the regular saccades (Figs. 7A and B). The sensor topographies of the SF of both saccade types were highly correlated ($r=0.86$). However, the SF of miniature saccades differed in amplitude from that of regular saccades. The average amplitude over frontal and temporal regions of interest was ~200% larger for regular saccades compared to miniature saccades (Fig. 7C; $p=3.6\times10^{-6}$, Bonferroni corrected for $n=2$ comparisons). In contrast, the SF revealed only small differences in amplitude between saccades of 5.5° and 11° (8% signal increase, $p=8.2\times10^{-4}$, Bonferroni corrected for $n=2$ comparisons). Similar to the SF, the average SP amplitude at frontal and parietal electrodes of interest was ~110% larger for regular compared to miniature saccades (Fig. 7D; $p=2.1\times10^{-5}$, Bonferroni corrected for $n=2$ comparisons). The difference in average SP amplitude between 11° and 5.5° saccades remained nonsignificant (5% signal increase for 11° saccades, $p=8.6\times10^{-2}$, Bonferroni corrected for $n=2$ comparisons).

Source analysis of the SF from miniature saccades revealed the strongest power changes at 64 Hz at the extraocular muscles behind the eyes (Fig. 8; $p<0.01$, FDR corrected). Thus, the source distribution of the SF from miniature saccades resembled the source distribution that we derived for regular saccades but with reduced amplitude (compare to Fig. 4B). In summary, the amplitude of the SF was modulated nonlinearly with saccade size but the spatial distribution at source and sensor level remained constant.

Discussion

We provide the first characterization of the saccadic spike field (SF), the saccadic spike artifact in MEG. Our results show that the saccadic spike artifact affects MEG signals mainly at frontal and temporal sensors. We observed that the topography of the SF is modulated with

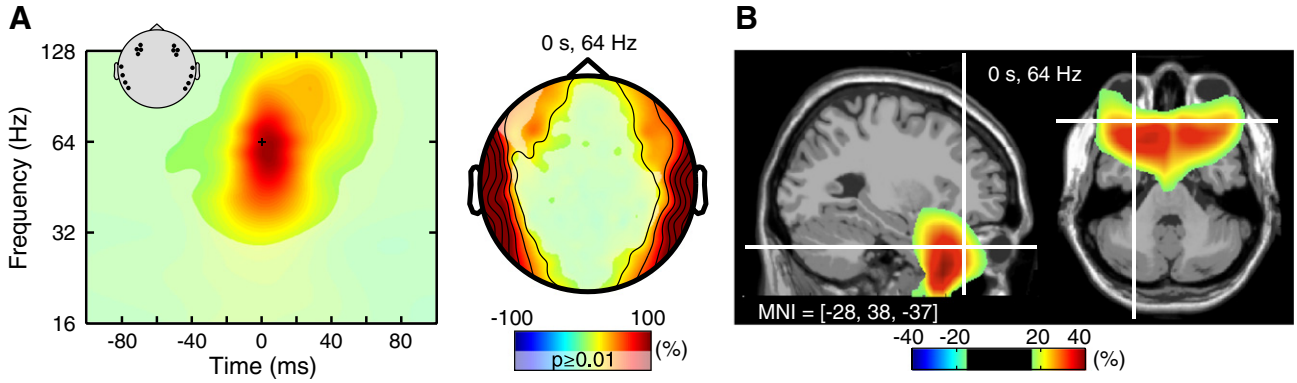

Fig. 4. Spectral characteristics of the SF. A. Power change at sensor level around the onset of saccades relative to baseline average from 400 ms to 350 ms before saccade onset. Unmasked regions denote significant difference to zero (*t*-test, $p<0.01$, FDR corrected). Left: power response resolved in time and frequency for selected regions of interest (indicated in the inset). Right: topography of the relative power changes for 64 Hz at saccade onset (time $t=0$ ms). Unmasked regions denote significant difference from zero (*t*-test, $p<0.01$, FDR corrected). B. Sources for the sensor topography shown in A overlaid on the MNI template brain. Data are masked by statistics (*t*-test, $p<0.01$, FDR corrected).

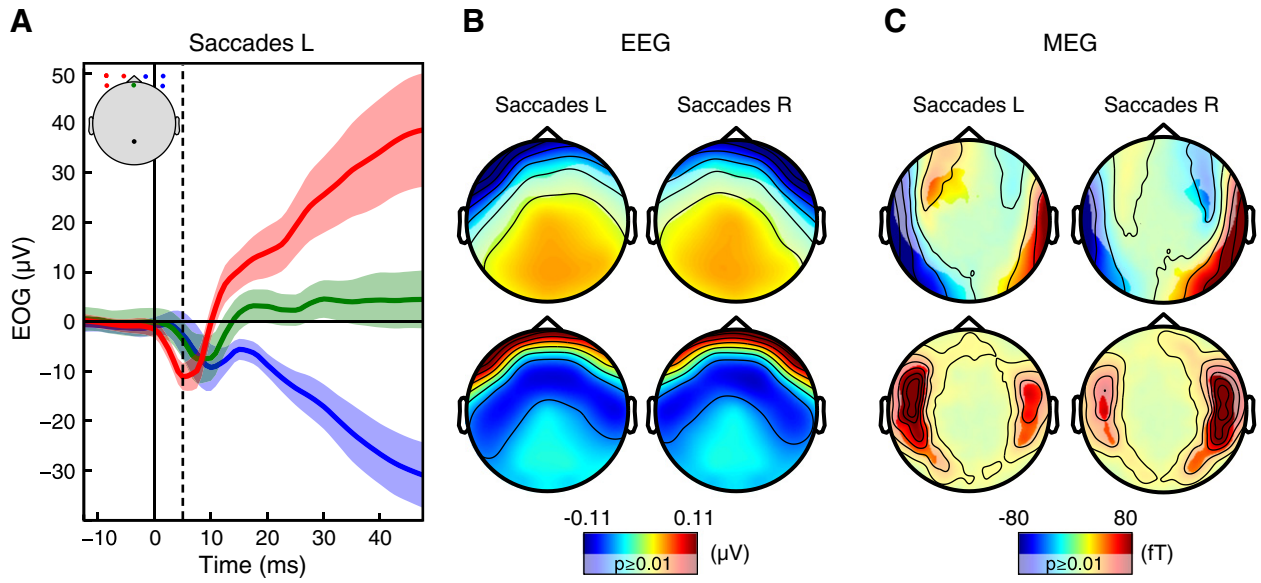

Fig. 5. Saccade direction reflected in SP and SF lateralization. A. Grand average time course of the SP around onset of leftwards saccades at different EOG sensors. The standard deviation is depicted in transparent shading. The inset shows the locations of EOG electrodes. As reference served electrode 'Pz' (black). B and C. Topographies of the SP/SF for leftwards and rightwards saccades respectively at the time of maximal lateralization (time t = 5 ms, dashed line in A). The signal at saccade onset (time t = 0 ms) was subtracted as baseline. All topographies except for the root-mean-square (B, lower panel) are statistically masked (*t*-test, $p<0.01$, Bonferroni corrected). B. SP in EEG. Top: event related signal. Bottom: root-mean-square. C. SF in MEG. Top: axial gradiometer representation. Bottom: planar gradiometer representation.

saccade direction while the SF amplitude depends on saccade size. Furthermore, our source analysis localizes the origin of the SF to the extraocular muscles. Because of its close resemblance to neural gamma band activity and its modulations in appearance and rate with experimental manipulations the saccadic spike artifact is prone to confusion with true neuronal activity in any EEG/MEG experiment. The detailed characterization of the SF in this study constitutes a solid basis for assessing possible saccadic spike related contamination in MEG experiments.

The saccadic spike in MEG and EEG

We found that the SF is a biphasic transient signal of ~24 ms duration and a peak-to-peak response of ~8 ms occurring at saccade onset. Its power spectrum is dominated by energy in the gamma frequency range (~32–128 Hz). With these properties it is consistent with the well-known SP in EEG (Keren et al., 2010a; Yuval-Greenberg et al., 2008). However, a crucial issue of great practical importance for the interpretation of the data is the difference in sensor topography. While the SF affects frontal and temporal MEG sensors, the SP has an impact on frontal and posterior EEG sensors. Both SF and SP are the measurement specific signatures of the saccadic spike produced with saccade initiation.

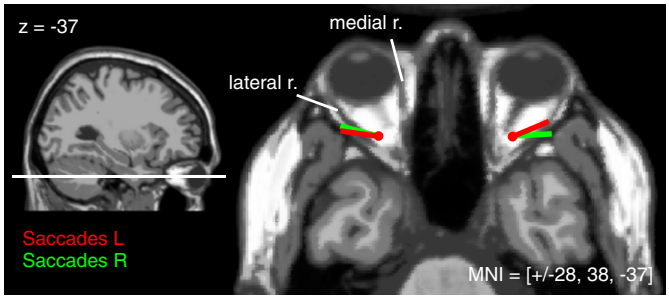

Fig. 6. Current dipoles for SF of saccades to left and right. Grand average dipole moments for fixed dipole positions at the center of the extraocular muscles rotate depending on the saccade directions. Dipoles were projected onto the nearest horizontal brain slice (MNI coordinate z = −37) for illustration. Red: average dipole direction for leftwards saccades. Green: same for rightwards saccades. Lateral r./medial r.: lateral/medial rectus muscle of the left eye.

Source localization confirms extraocular muscles as saccadic spike generator

Our results provide the first distributed source estimation of the saccadic spike field in MEG. We reliably localized the saccadic spike artifact of the miniature and regular saccades in the centers of the extraocular muscles of each eye. The source localization is robust with respect to different saccade types (miniature or regular saccades) and different signal representations (frequency or time domain). In accordance with the spatial resolution of MEG, the source reconstruction does not resolve individual muscles in the periorbital space but locates the source into the region spanned by the extraocular muscles of each eye. Nevertheless, the source estimation provides strong evidence for the muscular origin of the saccadic spike artifact arguing against any cortical contribution (Balaban and Weinstein, 1985; Brooks-Eidelberg and Adler, 1992; Csibra et al., 1997, 2000; Parks and Corballis, 2008). Our results substantiate previous EEG studies that suggested the myogenic origin of the saccadic spike artifact based on patient data and sensor characteristics of the saccadic spike (Becker et al., 1972; Blinn, 1955; Boylan and Doig, 1989b; Dimigen et al., 2009; Keren et al., 2010a; Moster and Goldberg, 1990; Picton et al., 2000; Riemslag et al., 1988; Thickbroom and Mastaglia, 1985, 1987) or provided constrained source models of the SP (Hassler et al., 2011; Picton et al., 2000; Thickbroom and Mastaglia, 1985; Yuval-Greenberg et al., 2008). Our findings further agree with evidence from intracranial recordings that observed the highest saccadic spike amplitudes in the temporal pole near the extraocular muscles (Jerbi et al., 2009; Kovach et al., 2011). In summary, our source estimation confirms that the saccadic spike reflects the engagement of the extraocular muscles at saccade onset. Furthermore, we show that the artifact can be reliably identified by distributed source analysis.

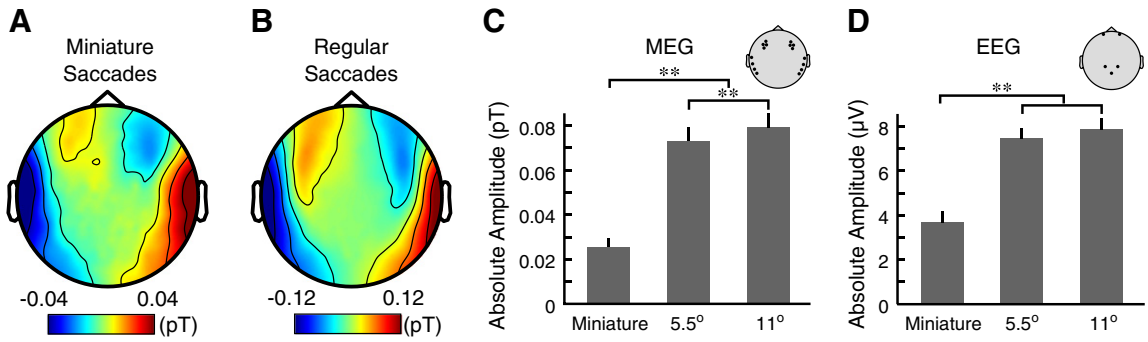

Fig. 7. The SF of miniature and regular saccades. A. Sensor topography of the SF for miniature saccades of less than 2° amplitude at the first peak of the saccadic spike (relative to baseline at saccade onset, axial gradiometers). B. Equivalent sensor topography for regular saccades (5.5° and 11° amplitude). C. Average absolute amplitude of the SF at sensors of interest (indicated in inset) for different saccade sizes (**t-test, $p<0.01$, Bonferroni corrected). Bars indicate the standard error. D. Average absolute amplitude of the SP at sensors of interest (indicated in inset) for different saccade sizes (**t-test, $p<0.01$, Bonferroni corrected).

Modulation of SF with saccade metrics

Even in experiments demanding steady fixation, experimental stimulus and task parameters can influence the size (Gowen et al., 2005; Yuval-Greenberg et al., 2008) and direction (Engbert and Kliegl, 2003; Gowen et al., 2007; Laubrock et al., 2010; Rolfs et al., 2004; Turatto et al., 2007) of fixational eye movements. Consequently, understanding the modulation of SF with saccade metrics is necessary to assess the effect of SF artifacts in experiments with asymmetric saccade statistics.

Our results show, that the SF in MEG is enhanced ipsilateral to saccade direction. The effect is strongest at temporal sensors. These findings are consistent with the lateralized topography of the saccadic spike that we and others observed in EEG (Keren et al., 2010a; Kovach et al., 2011; Moster and Goldberg, 1990; Moster et al., 1997; Thickbroom and Mastaglia, 1985, 1986). It has been suggested that the saccadic spike reflects the summation potential of synchronously recruited motor units of the extraocular muscles (Blinn, 1955; Moster and Goldberg, 1990; Picton et al., 2000; Thickbroom and Mastaglia, 1985). Building on our beamforming results, we demonstrate that a dipole model of the lateralized SF is indeed compatible with the asymmetrical contraction pattern of the predominantly engaged muscles during horizontal saccades, namely, the ipsilateral rectus lateralis and contralateral rectus medialis muscle.

We expect similar saccadic spike topographies for horizontal saccades that are performed from peripheral locations of the visual field towards the center. These saccades engage the same muscles as the centrifugal saccades we observed but with a different contraction level before saccade onset, affecting probably the amplitude of the saccadic spike. Saccades in directions other than the horizontal plane require the participation of different extraocular muscles, which presumably slightly changes the topography of the SF as indicated by previous EEG studies (Keren et al., 2010a; Thickbroom and Mastaglia, 1986).

The SF for saccades of different amplitudes did not differ in sensor topography or the distribution of sources. However, we found strongly reduced SF amplitudes for miniature saccades compared to the 5.5° and 11° saccades, but only minor amplitude differences between both types of regular saccades. We found a similar relation for EEG except that the difference between both types of regular saccades did not reach significance. These results are in line with previous EEG studies, supporting a nonlinear dependence of saccade size on saccadic spike amplitude (Armington, 1978; Boylan and Doig, 1989b; Keren et al., 2010a; Kovach et al., 2011; Riemslag et al., 1988; Thickbroom and Mastaglia, 1985). These studies observed an amplitude dependence for saccades up to 10° while the amplitude of the saccadic spike remained constant for larger saccades. Most probably, the maximal recruitment of motor units is already reached for these large saccades (Thickbroom and Mastaglia, 1987). The similarity of the sensor topography and source localization of the SF for spontaneous miniature and guided regular saccades suggests that both types of saccades have the same muscular recruitment pattern and thus the same sources underlying their saccadic spike artifact.

In summary, our results show that saccade metrics affect the topography and amplitude of both the SF and the SP in a characteristic manner. Any experimental comparison that may be accompanied by asymmetric saccade patterns could therefore be subject to a potential confound with metric specific changes of the saccadic spike artifact and should be carefully controlled.

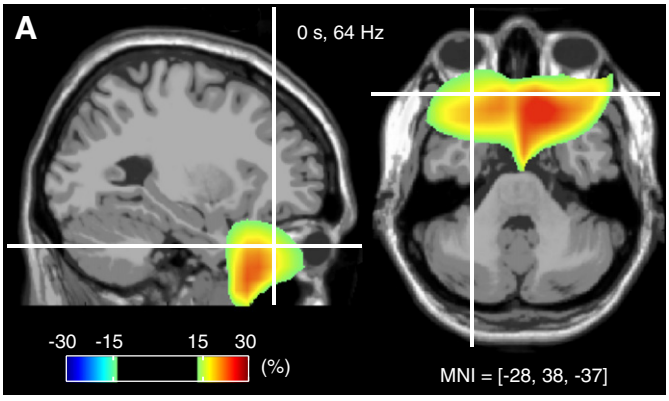

Fig. 8. Source analysis of SF from miniature saccades. Source of the relative change in signal power at 64 Hz at saccade onset compared to average baseline at 135 ms to 85 ms before miniature saccade onset. Functional data are overlaid on the MNI template brain and statistically masked (t-test, $p<0.01$, FDR corrected).

Practical implications for MEG experiments

In contrast to EEG, the saccadic spike artifact in MEG does not affect posterior sensors. Consequently, the SF is not prone to misinterpretations as gamma activity reflecting higher visual processes in parietal and occipital areas, as it is the case for EEG (Yuval-Greenberg et al., 2008). However, the SF may be confused with neuronal activity originating from frontal and temporal brain regions. For example, the response to auditory stimulation at the MEG sensor level might be contaminated by saccadic spike induced gamma band responses in the temporal cortex. The miniature saccade rate is characteristically modulated by auditory stimulation and additionally

depends on experimental manipulations. Consequently, auditory stimulation can lead to task modulated gamma band responses due to the saccadic spike artifact (Yuval-Greenberg and Deouell, 2011). For auditory MEG experiments, the SF artifact could then confound genuine neural responses within the auditory processing stream since both map to overlapping temporal MEG sensors. Similarly, any neural activity reflecting higher cognitive processing in temporal and prefrontal cortex that maps to similar sensors as the SF might be subject to artifact contamination from the saccadic spike. Thus, unlike the SP in EEG, the SF in MEG is not prone to confusion with neuronal activity in parietal and occipital cortex, but putative frontal and temporal neuronal processes need to be carefully controlled for the saccadic spike artifact. It should be further noted, that for some analyses artifacts could have consequences far beyond their topographical maximum. For example when computing measures of neuronal interactions such as phase synchronization between sensors the saccadic spike artifact may be problematic for a large part of all sensors.

To control for saccadic spike artifacts the first step is to investigate the modulation of the saccadic spike rate along with the experimental contrast at hand. Saccades and miniature saccades can be measured via video based eye tracking along with MEG/EEG but this is technically challenging and often the equipment is not available. An efficient and practical alternative is to follow the procedure described by Keren et al. (2010a) that detects SPs in the REOG. Importantly, to apply this approach in MEG experiments a parietal reference electrode is needed to measure the REOG. We highly recommend adapting this as a standard procedure in MEG experiments. If the saccadic spike rate is indeed modulated along with the experimental contrast, putative effects of neuronal origin need to be critically evaluated. Our characterization of the SF provides a reference for this purpose. The precise comparison of the temporal, spatial and spectral characteristics of the signal of interest with the characteristics of the saccadic spike artifact may help to clarify the origin.

If the saccadic spike artifact covers potential neural signatures artifact cleaning and separation procedures are required. Our investigations provide a starting point for future studies exploring artifact cleaning procedures on the removal of the saccadic spike artifact in MEG. Promising candidates are independent component analysis or linear regression techniques that have successfully been applied in EEG to remove saccadic spike artifacts (Hassler et al., 2011; Keren et al., 2010a; Kovach et al., 2011; Nottage, 2010).

However, most cleaning procedures only augment the signal-to-noise ratio without perfectly separating noise from genuine neural signals (Keren et al., 2010a; Nottage, 2010; Shackman et al., 2010) and should therefore not replace a careful identification and visualization of the artifact. As an alternative to these procedures, we suggest an analysis in source space. Beamforming is especially well suited for separating artifacts from cortical sources, because it does not rely on inverse solutions. Hence, beamforming does not assume cortical sources for the entire sensor signal containing putative artifacts (Baillet et al., 2001). We showed that beamforming reliably locates the SF in the extraorbital region. While neuronal activity in the orbitofrontal cortex or the temporal pole may still be difficult to disentangle from the artifact, our results provide evidence that beamforming is suitable for spatially separating the saccadic spike artifact from neuronal signals if the latter is sufficiently distant from the former.

Acknowledgments

We thank Constanze Hipp for helpful comments on the manuscript. This work was supported by grants from the European Union (IST-2005-027268, NEST-PATH-043457, HEALTH-F2-2008-200728, FP7-ICT-270212, ERC-2010-AdG-269716) and the German Federal Ministry of Education and Research (Neuroimage Nord).

References

Armington, J.C., 1978. Potentials that precede small saccades. In: Armington, J.C., Krauskopf, J., Wooten, B.R. (Eds.), Visual Psychophysics and Physiology. Academic Press, New York, pp. 363–372.
Baillet, S., Mosher, J.C., Leahy, R.M., 2001. Electromagnetic brain mapping. Signal Process. Mag. IEEE 18 (6), 14–30.
Balaban, C.D., Weinstein, J.M., 1985. The human pre-saccadic spike potential: influences of a visual target, saccade direction, electrode laterality and instructions to perform saccades. Brain Res. 347 (1), 49–57.
Bastiaansen, M.C., Knösche, T.R., 2000. Tangential derivative mapping of axial MEG applied to event-related desynchronization research. Clin. Neurophysiol. 111 (7), 1300–1305.
Becker, W., Hoehne, O., Iwase, K., Kornhuber, H., 1972. Bereitschaftspotential, prämotorische Positivierung und andere Hirnpotentiale bei sakkadischen Augenbewegungen. Vision Res. 12, 421–436.
Benjamini, Y., Hochberg, Y., 1995. Controlling the false discovery rate: a practical and powerful approach to multiple testing. J. R. Stat. Soc. Series B Stat. Methodol. 57 (1), 289–300.
Blinn, K.A., 1955. Focal anterior temporal spikes from external rectus muscle. EEG Clin. Neurophysiol. 7 (2), 299–302.
Boylan, C., Doig, H.R., 1989a. Presaccadic spike potential with congenital lateral rectus palsy. EEG Clin. Neurophysiol. 73 (3), 264–267.
Boylan, C., Doig, H.R., 1989b. Effect of saccade size on presaccadic spike potential amplitude. Invest. Ophthalmol. Vis. Sci. 30 (12), 2521–2527.
Brookes, M.J., Stevenson, C.M., Barnes, G.R., Hillebrand, A., Simpson, M.I.G., Francis, S.T., Morris, P.G., 2007. Beamformer reconstruction of correlated sources using a modified source model. Neuroimage 34 (4), 1454–1465.
Brooks-Eidelberg, B.A., Adler, G., 1992. A frontal cortical potential associated with saccades in humans. Exp. Brain Res. 89 (2), 441–446.
Csibra, G., Johnson, M.H., Tucker, L.A., 1997. Attention and oculomotor control: a high-density ERP study of the gap effect. Neuropsychologia 35 (6), 855–865.
Csibra, G., Tucker, L.A., Volein, A., Johnson, M.H., 2000. Cortical development and saccade planning: the ontogeny of the spike potential. Neuroreport 11 (5), 1069–1073.
Dalal, S.S., Sekihara, K., Nagarajan, S.S., 2006. Modified beamformers for coherent source region suppression. IEEE Trans. Biomed. Eng. 53 (7), 1357–1363.
Dimigen, O., Valsecchi, M., Sommer, W., Kliegl, R., 2009. Human microsaccade-related visual brain responses. J. Neurosci. 29 (39), 12321–12331.
Engbert, R., 2006. Microsaccades: a microcosm for research on oculomotor control, attention, and visual perception. Prog. Brain Res. 154, 177–192.
Engbert, R., Kliegl, R., 2003. Microsaccades uncover the orientation of covert attention. Vision Res. 43 (9), 1035–1045.
Fries, P., Scheeringa, R., Oostenveld, R., 2008. Finding gamma. Comments to Yuval-Greenberg. Neuron 58 (3), 303–305.
Genovese, C.R., Lazar, N.A., Nichols, T., 2002. Thresholding of statistical maps in functional neuroimaging using the false discovery rate. Neuroimage 15 (4), 870–878.
Gowen, E., Abadi, R.V., Poliakoff, E., 2005. Paying attention to saccadic intrusions. Cogn. Brain Res. 25 (3), 810–825.
Gowen, E., Abadi, R.V., Poliakoff, E., Hansen, P.C., Miall, R.C., 2007. Modulation of saccadic intrusions by exogenous and endogenous attention. Brain Res. 1141, 154–167.
Gross, J., Kujala, J., Hamalainen, M., Timmermann, L., Schnitzler, A., Salmelin, R., 2001. Dynamic imaging of coherent sources: studying neural interactions in the human brain. Proc. Natl. Acad. Sci. U. S. A. 98 (2), 694–699.
Gruber, T., 2008. It's all in your eyes? Induced gamma band responses in the human EEG. Comment on Yuval-GreenbergNeuron Online Comments http://www.cell.com/neuron/viewComment/S0896-6273(08)00301-2.
Hämäläinen, M.S., 1995. Functional localization based on measurements with a whole-head magnetometer system. Brain Topogr. 7 (4), 283–289.
Hämäläinen, M., Hari, R., Ilmoniemi, R.J., Knuutila, J., Lounasmaa, O.V., 1993. Magnetoencephalography—theory, instrumentation, and applications to noninvasive studies of the working human brain. Rev. Mod. Phys. 65 (2), 413–497.
Hassler, U., Trujillo Barreto, N., Gruber, T., 2011. Induced gamma band responses in human EEG after the control of miniature saccadic artifacts. Neuroimage 57 (4), 1411–1421.
Hipp, J.F., Engel, A.K., Siegel, M., 2011. Oscillatory synchronization in large-scale cortical networks predicts perception. Neuron 69 (2), 387–396.
Holmes, C.J., Hoge, R., Collins, L., Woods, R., Toga, A.W., Evans, A.C., 1998. Enhancement of MR images using registration for signal averaging. J. Comput. Assist. Tomogr. 22 (2), 324–333.
Jagla, F., Jergelová, M., Riecanský, I., 2007. Saccadic eye movement related potentials. Physiol. Res. / Acad. Sci. Bohemoslov. 56 (6), 707–713.
Jerbi, K., Freyermuth, S., Dalal, S., Kahane, P., Bertrand, O., Berthoz, A., Lachaux, J.-P., 2009. Saccade related gamma-band activity in intracerebral EEG: dissociating neural from ocular muscle activity. Brain Topogr. 22 (1), 18–23.
Keren, A.S., Yuval-Greenberg, S., Deouell, L.Y., 2010a. Saccadic spike potentials in gamma-band EEG: characterization, detection and suppression. Neuroimage 49 (3), 2248–2263.
Keren, A.S., Yuval-Greenberg, S., Gao, Z., Gerber, E., Bentinand, S., Deouell, L.Y., 2010b. Saccadic spike potentials in gamma-band EEG and MEG: characterization, detection and suppression. Human Brain Mapping Annual Meeting, Barcelona. Abstract no. 1014 WTh-PM.
Kovach, C.K., Tsuchiya, N., Kawasaki, H., Oya, H., Howard III, M.A., Adolphs, R., 2011. Manifestation of ocular-muscle EMG contamination in human intracranial recordings. Neuroimage 54 (1), 213–233.

Kurtzberg, D., Vaughan, H.G., 1982. Topographic analysis of human cortical potentials preceding self-initiated and visually triggered saccades. Brain Res. 243, 1–9.
Laubrock, J., Engbert, R., Kliegl, R., 2005. Microsaccade dynamics during covert attention. Vision Res. 45 (6), 721–730.
Laubrock, J., Engbert, R., Kliegl, R., 2008. Fixational eye movements predict the perceived direction of ambiguous apparent motion. J. Vis. 8 (14), 1–17.
Laubrock, J., Kliegl, R., Rolfs, M., Engbert, R., 2010. When do microsaccades follow spatial attention? Atten. Percept. Psychophys. 72 (3), 683–694.
Martinez-Conde, S., 2006. Fixational eye movements in normal and pathological vision. Prog. Brain Res. 154, 151–176.
Martinez-Conde, S., Macknik, S.L., Troncoso, X.G., Hubel, D.H., 2009. Microsaccades: a neurophysiological analysis. Trends Neurosci. 32 (9), 463–475.
Moster, M.L., Goldberg, G., 1990. Topography of scalp potentials preceding self-initiated saccades. Neurology 40 (4), 644–648.
Moster, M.L., Roemer, R.A., Shagass, C., Polansky, M., Shan, Y., 1997. Presaccadic spike potential in normal subjects. Neuroophthalmology 18 (4), 185–190.
Nichols, T.E., Holmes, A.P., 2002. Nonparametric permutation tests for functional neuroimaging: a primer with examples. Hum. Brain Mapp. 15 (1), 1–25.
Nolte, G., 2003. The magnetic lead field theorem in the quasi-static approximation and its use for magnetoencephalography forward calculation in realistic volume conductors. Phys. Med. Biol. 48 (22), 3637–3652.
Nottage, J.F., 2010. Uncovering gamma in visual tasks. Brain Topogr. 23 (1), 58–71.
Oostenveld, R., Fries, P., Maris, E., Schoffelen, J.M., 2011. FieldTrip: open source software for advanced analysis of MEG, EEG, and invasive electrophysiological data. Comput. Intell. Neurosci. 2011 (156869), 1–9.
Parks, N.A., Corballis, P.M., 2008. Electrophysiological correlates of presaccadic remapping in humans. Psychophysiology 45 (5), 776–783.
Picton, T.W., van Roon, P., Armilio, M.L., Berg, P., Ille, N., Scherg, M., 2000. Blinks, saccades, extraocular muscles and visual evoked potentials (reply to Verleger). J. Psychophysiol. 14, 210–217.
Reingold, E.M., Stampe, D.M., 2002. Saccadic inhibition in voluntary and reflexive saccades. J. Cogn. Neurosci. 14 (3), 371–388.
Reva, N.V., Aftanas, L.I., 2004. The coincidence between late non-phase-locked gamma synchronization response and saccadic eye movements. Int. J. Psychophysiol. 51, 215–222.
Riemslag, F.C., Van der Heijde, G.L., Van Dongen, M.M., Ottenhoff, F., 1988. On the origin of the presaccadic spike potential. EEG Clin. Neurophysiol. 70 (4), 281–287.
Rolfs, M., 2009. Microsaccades: small steps on a long way. Vision Res. 49 (20), 2415–2441.
Rolfs, M., Engbert, R., Kliegl, R., 2004. Microsaccade orientation supports attentional enhancement opposite a peripheral cue: commentary on Tse, Sheinberg, and Logothetis (2003). Psychol. Sci. 15 (10), 705–707 author reply 708–710.
Rolfs, M., Kliegl, R., Engbert, R., 2008. Toward a model of microsaccade generation: the case of microsaccadic inhibition. J. Vis. 8 (11), 1–23.
Salvucci, D.D., Goldberg, J.H., 2000. Identifying fixations and saccades in eye-tracking protocols. Proceedings of the Symposium on Eye Tracking Research & Applications — ETRA '00, Florida, pp. 71–78.
Schwartzman, D.J., Kranczioch, C., 2011. In the blink of an eye: the contribution of microsaccadic activity to the induced gamma band response. Int. J. Psychophysiol. 79 (1), 73–82.
Shackman, A.J., McMenamin, B.W., Maxwell, J.S., Greischar, L.L., Davidson, R.J., 2010. Identifying robust and sensitive frequency bands for interrogating neural oscillations. Neuroimage 51 (4), 1319–1333.
Tallon-Baudry, C., Bertrand, O., Delpuech, C., Pernier, J., 1996. Stimulus specificity of phase-locked and non-phase-locked 40 Hz visual responses in human. J. Neurosci. 16 (13), 4240–4249.
Thickbroom, G.W., Mastaglia, F.L., 1985. Presaccadic 'spike' potential: investigation of topography and source. Brain Res. 339 (2), 271–280.
Thickbroom, G.W., Mastaglia, F.L., 1986. Presaccadic spike potential. Relation to eye movement direction. EEG Clin. Neurophysiol. 64 (3), 211–214.
Thickbroom, G.W., Mastaglia, F.L., 1987. Presaccadic spike potential: a computer model based upon motor unit recruitment patterns in the extraocular muscles. Brain Res. 422 (2), 377–380.
Troncoso, X.G., Macknik, S.L., Otero-Millan, J., Martinez-Conde, S., 2008. Microsaccades drive illusory motion in the Enigma illusion. Proc. Natl. Acad. Sci. U. S. A. 105 (41), 16033–16038.
Trujillo, L.T., Peterson, M.A., Kaszniak, A.W., Allen, J.J.B., 2005. EEG phase synchrony differences across visual perception conditions may depend on recording and analysis methods. Clin. Neurophysiol. 116, 172–189.
Turatto, M., Valsecchi, M., Tamè, L., Betta, E., 2007. Microsaccades distinguish between global and local visual processing. Neuroreport 18 (10), 1015–1018.
Valsecchi, M., Betta, E., Turatto, M., 2007. Visual oddballs induce prolonged microsaccadic inhibition. Exp. Brain Res. 177 (2), 196–208.
Valsecchi, M., Dimigen, O., Kliegl, R., Sommer, W., Turatto, M., 2009. Microsaccadic inhibition and P300 enhancement in a visual oddball task. Psychophysiology 46 (3), 635–644.
Van Dam, L.C.J., van Ee, R., 2006. Retinal image shifts, but not eye movements per se, cause alternations in awareness during binocular rivalry. J. Vis. 6 (11), 1172–1179.
Van Veen, B.D., van Drongelen, W., Yuchtman, M., Suzuki, A., 1997. Localization of brain electrical activity via linearly constrained minimum variance spatial filtering. IEEE Trans. Biomed. Eng. 44, 867–880.
Yuval-Greenberg, S., Deouell, L.Y., 2011. Scalp-recorded induced gamma-band responses to auditory stimulation and its correlations with saccadic muscle activity. Brain Topogr. 24 (1), 30–39.
Yuval-Greenberg, S., Tomer, O., Keren, A.S., Nelken, I., Deouell, L.Y., 2008. Transient induced gamma-band response in EEG as a manifestation of miniature saccades. Neuron 58, 429–441.